submitted to *Geophys. J. Int.*

Rapid and simultaneous estimation of fault slip and heterogeneous lithospheric viscosity from postseismic deformation

T.T. Hines[1] and E.A. Hetland[1]

[1] *University of Michigan, Ann Arbor, MI, USA*

SUMMARY

Postseismic deformation is commonly attributed to viscoelastic relaxation and/or afterslip, although discerning between the two driving mechanisms can be difficult. A major complication in modeling postseismic deformation is that forward models can be computationally expensive, making it difficult to adequately search model space to find the optimal fault slip distribution and lithospheric viscosity structure that can explain observable postseismic deformation. We propose an inverse method which uses coseismic and early postseismic deformation to rapidly and simultaneously estimate a fault slip history and an arbitrarily discretized viscosity structure of the lithosphere. Our method is based on an approximation which is applicable to the early postseismic period and expresses surface deformation resulting from viscoelastic relaxation as a linearized function with respect to lithospheric fluidity. We demonstrate this approximation using two-dimensional earthquake models. We validate the approximation and our inverse method using two three-dimensional synthetic tests. The success of our synthetic tests suggests that our method is capable of distinguishing the mechanisms driving early postseismic deformation and recovering an effective viscosity structure of the lithosphere.

Key words: Seismic cycle, Inverse theory, Rheology: crust and lithosphere, Transient deformation

1 INTRODUCTION

Geodetic observations of surface deformation in the months to years following an earthquake are often attributed to afterslip (e.g. Marone et al. 1991), viscoelastic relaxation in the lithosphere (e.g. Nur & Mavko 1974), and/or poroelastic relaxation (e.g. Peltzer et al. 1998). If postseismic deformation can be entirely described by afterslip, then one could easily constrain the spatial distribution of slip on prescribed fault geometries with a linear least squares inversion (e.g. Harris & Segall 1987; Bürgmann et al. 2002; Freed 2007), which could then provide insight into the frictional properties of faults (e.g. Hsu et al. 2006; Barbot et al. 2009). However, postseismic deformation following large ($M_w \geq 7$) earthquakes is often attributed to viscoelastic relaxation in the lithosphere (e.g. Hetland & Hager 2003; Pollitz 2003, 2005) or a combination of both afterslip and viscoelastic relaxation (e.g. Freed et al. 2006a; Hearn et al. 2009; Johnson et al. 2009; Rollins et al. 2015). In such cases, postseismic deformation can be used to also constrain the viscous properties of the lithosphere, although this is a more difficult task than constraining just a slip distribution. Not only do the competing deformation mechanism need to be discerned, finding the viscosity distribution of the lithosphere from postseismic deformation is a computationally expensive nonlinear inverse problem. Typically, the estimation of viscosities is approached with a forward modeling, grid search or Monte Carlo method. These forward modeling techniques require the number of unknown parameters being estimated to be small, meaning that significant and potentially inappropriate modeling assumptions must be made. Namely, studies seeking to estimate the viscosity structure of the lithosphere often assume for computational tractability that the lithosphere is composed of two or three homogeneously viscoelastic layers, which may not be appropriate for describing a more realistic depth dependent viscosity structure (Riva & Govers 2008; Hines & Hetland 2013).

In this paper we propose a relatively fast method to invert coseismic and postseismic deformation to simultaneously estimate a time-dependent distribution of fault slip and an arbitrarily discretized viscosity structure of the lithosphere. Our method is based on an approximation which linearizes the rate of early postseismic deformation with respect to the viscosity of the lithosphere. We demonstrate the effectiveness and limitations of our method through two synthetic tests.

2 APPROXIMATION FOR POSTSEISMIC DEFORMATION

We assume that the lithosphere can be approximated as a Maxwell viscoelastic material on the timescales of postseismic deformation, where shear stress, $\boldsymbol{\sigma}$, and strain, $\boldsymbol{\varepsilon}$, are related by

$$\frac{\partial \boldsymbol{\varepsilon}}{\partial t} = \frac{\boldsymbol{\sigma}}{2\eta} + \frac{1}{2\mu}\frac{\partial \boldsymbol{\sigma}}{\partial t}. \tag{1}$$

We use η and μ to represent viscosity and shear modulus, respectively. This constitutive relationship implies that a sudden strain from an earthquake will instantaneously stress the lithosphere elastically (assuming the lithosphere is undergoing quasi-static deformation). Viscoelastic creep will initiate immediately after the earthquake, where the initial viscous strain rate in each parcel of the lithosphere will be proportional to the fluidity ($1/\eta$) in that parcel, and independent of the fluidity elsewhere because the initial stresses are only controlled by the elastic properties of the lithosphere. Stresses from the earthquake will dissipate over time through viscoelastic relaxation. During the period in which stress changes from viscoelastic relaxation are small compared to the initial elastic stresses, each parcel will continue to creep at a rate that is approximately proportional to its fluidity. In this early postseismic period, the surface deformation from creep in each parcel will have an amplitude that is also proportional to the fluidity in that parcel and independent of the fluidity elsewhere. As we will show, the early surface expression of creep in the entire lithosphere is therefore a sum of the surface deformation from each parcel and is linear with respect to lithospheric fluidity. We demonstrate this property of early postseismic surface deformation in this section using simple infinite length, strike-slip earthquake models, where the lithosphere is approximated as a layered half-space. In Section 4 we consider two finite fault models with an arbitrarily discretized lithospheric viscosity structure, the first with only Maxwell viscoelasticity and the second with Burgers viscoelasticity.

2.1 Two-dimensional earthquake models

The easiest way to demonstrate how postseismic deformation can be linearized with respect to lithospheric viscosity is with a two-dimensional earthquake model consisting of a long, vertical, surface rupturing, strike-slip fault that is embedded in a viscoelastic horizontal layer overlying a viscoelastic half-space. We make use of the Correspondence Principle of Viscoelasticity (e.g. Flügge 1975), which states that the Laplace transform of deformation in a viscoelastic body has the same form as the Laplace transform of deformation in a elastic body with the same geometry and subjected to the same boundary conditions. The solution for displacements following an earthquake in a viscoelastic lithosphere can then be readily found provided that the corresponding elastic solution is known (e.g. Nur & Mavko 1974; Savage & Prescott 1978; Hetland & Hager 2005). One only needs to replace the shear modulus in the Laplace transform of the elastic solution with the effective viscoelastic shear modulus and then compute the inverse Laplace transform.

2.1.1 Two layered model

From the solution of Rybicki (1971), surface displacements, $u_e(x,t)$, resulting from slip on a fault in an elastic surface layer overlying a semi-infinite elastic substrate are

$$u_e(x,t) = b(t)\left(\frac{1}{2}W(0) + \sum_{n=1}^{\infty}\Gamma^n W(n)\right), \tag{2}$$

where

$$W(n) = \frac{1}{\pi}\left(\tan^{-1}\left(\frac{2nH+D}{x}\right) - \tan^{-1}\left(\frac{2nH-D}{x}\right)\right) \tag{3}$$

and

$$\Gamma = \frac{\mu_1 - \mu_2}{\mu_1 + \mu_2}. \tag{4}$$

In the above equation, $b(t)$ describes cumulative slip on the fault through time and can describe co-seismic slip and/or afterslip. D is the locking depth of the fault, H is the thickness of the upper layer, and μ_1 and μ_2 are the shear moduli in the upper layer and lower substrate, respectively. The Laplace transform of eq. (2) is

$$\hat{u}_e(x,s) = \hat{b}(s)\left(\frac{1}{2}W(0) + \sum_{n=1}^{\infty}\Gamma^n W(n)\right). \tag{5}$$

We replace μ_1 and μ_2 in eq. (5) with the equivalent shear moduli for Maxwell materials in the Laplace domain, $\hat{\mu}_1$ and $\hat{\mu}_2$, to get the Laplace transform of surface displacements in the two-layered, viscoelastic half-space,

$$\hat{u}_v(x,s) = \hat{b}(s)\left(\frac{1}{2}W(0) + \sum_{n=1}^{\infty}\hat{\Gamma}^n W(n)\right), \tag{6}$$

where

$$\hat{\Gamma} = \frac{\hat{\mu_1} - \hat{\mu_2}}{\hat{\mu_1} + \hat{\mu_2}} \tag{7}$$

and

$$\hat{\mu_i} = \frac{s}{\frac{s}{\mu_i} + \frac{1}{\eta_i}}. \tag{8}$$

To find the surface displacements in the time domain one must find the inverse Laplace transform of eq. (6), which is typically done using the method of residues. However, we are interested in characterizing the behavior of only the early postseismic deformation and it serves us better to instead perform the inverse Laplace transform with an extension of the initial value theorem (Appendix A). We assume for simplicity that the shear modulus for the viscoelastic lithosphere is homogeneous (i.e. $\mu_1 = \mu_2$) and demonstrate in a supplementary IPython notebook that our conclusions still hold when $\mu_1 \neq \mu_2$.

The surface displacements in the time domain are

$$u_v(x,t) = b(t)\frac{1}{2}W(0) + b(t) * \mathcal{L}^{-1}\left[\sum_{n=1}^{\infty}\hat{\Gamma}^n W(n)\right], \tag{9}$$

where we use $*$ to denote a convolution with respect to time. Evaluating the above inverse Laplace transform using the method described in Appendix A, we find

$$\begin{aligned} u_v(x,t) =& b(t)\frac{1}{2}W(0)+ \\ & b(t) * \left(\frac{\mu}{2\eta_2}W(1) - \frac{\mu}{2\eta_1}W(1)\right) + \\ & b(t) * \left(\left(\frac{\mu^2 t}{4\eta_2^2} - \frac{\mu^2 t}{4\eta_1\eta_2}\right)(W(1) - W(2)) + \left(\frac{\mu^2 t}{4\eta_1\eta_2} - \frac{\mu^2 t}{4\eta_1^2}\right)(W(1) + W(2))\right) + \\ & \ldots . \end{aligned} \tag{10}$$

The first term in eq. (10) is the elastic response to slip on the fault. The remaining terms describe the surface displacement due to viscoelastic relaxation. We refer to the first of these remaining terms as the initial viscoelastic response, which describes surface deformation resulting from viscoelastic creep during the period in which the stresses from fault slip are unaltered by viscoelastic relaxation. The initial viscoelastic response is linear with respect to the fluidity in each of the two layers.

If the time since the rupture is sufficiently small compared to the relaxation times of each layer, $\tau_i = \eta_i/\mu$, (i.e. the third and following terms in eq. (10) are small) and the timescale of slip described by $b(t)$ is also short compared to the relaxation times in the half-space, then we can truncate the series and approximate early surface deformation using only the elastic response and the initial viscoelastic response,

$$u_v(x,t) \approx b(t)\frac{1}{2}W(0) + \int_0^t b(\theta)\left(\frac{\mu}{2\eta_2}W(1) - \frac{\mu}{2\eta_1}W(1)\right)d\theta. \tag{11}$$

An approximation similar to eq. (11) was demonstrated by Segall (2010) for an elastic layer over a Maxwell viscoelastic substrate.

Fig. 1 shows the series solution from eq. (10) truncated after sufficiently many terms along with the approximation given by eq. (11). In this comparison, we use $H = 15$ km, $D = 10$ km and a shear modulus of 32 GPa throughout the lithosphere. The upper layer is given a viscosity of 10^{20} Pa s ($\tau \approx 100$ years) and the substrate is given a viscosity of 10^{19} Pa s ($\tau \approx 10$ years). We let $b(t)$ describe a unit of instantaneous slip at $t = 0$. In the series solution, the rate of surface deformation decreases over time as stresses in the half-space decay through viscoelastic relaxation. Because $b(t)$ is a constant after $t = 0$, the initial viscoelastic response in eq. (11) describes a constant rate of surface deformation and so eq. (11) is a good approximation for as long as the rate of deformation predicted by eq. (10) is also approximately constant. We find the that the approximation is indistinguishable

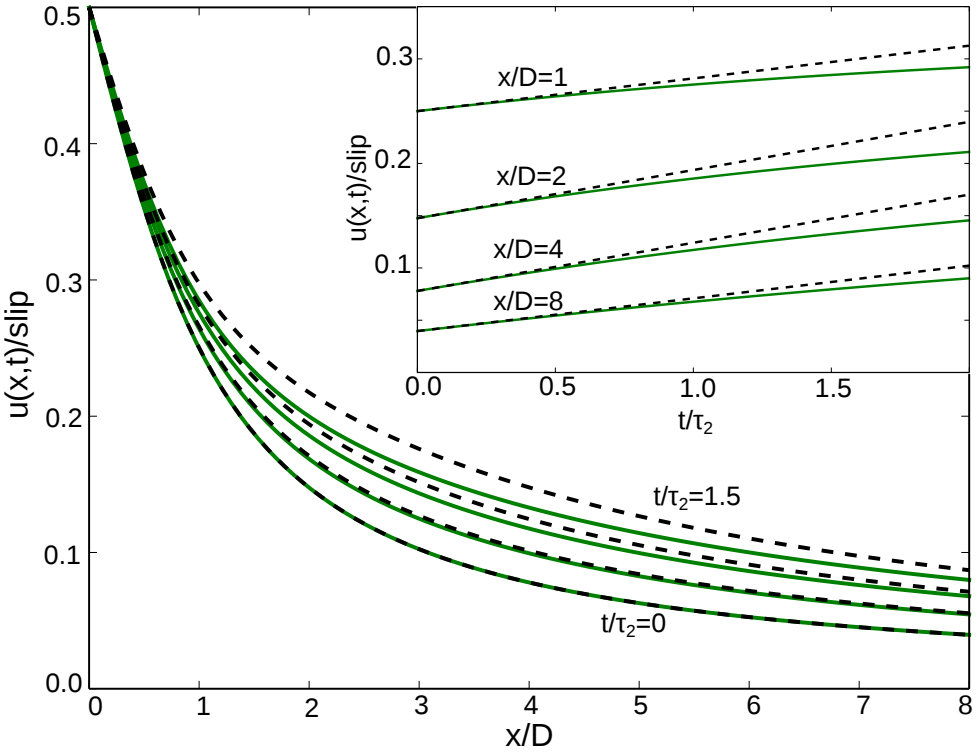

Figure 1. Surface displacements predicted by eq. (10) truncated after ten terms (green) and the approximation given by eq. (11) (dotted black). Times are normalized by the lowest relaxation time in the lithosphere, τ_2, and distances are normalized by the fault locking depth, D. Displacements are shown as a function of distance from the fault at times $t/\tau_2 = 0.0, 0.5, 1.0$ and 1.5. The inset figure shows displacement time series at locations $x/D = 1, 2, 4$ and 8.

from the series solution for at least as long as half the lowest of the two relaxation times, regardless of our choice of model parameters. The approximation breaks down faster than what is show in Fig. 1 when the upper layer is more fluid than the substrate or when we decrease the depth of the material interface (i.e. when the more fluid material is closer to the fault). We also note that the approximation has more longevity for locations further away from the fault, where it starts to break down at about the minimum relaxation time in the lithosphere.

2.1.2 Three layered and continuous depth dependent models

We follow the same procedure as above to find the surface deformation resulting from slip on a strike-slip fault in a three layered viscoelastic half-space. Starting from the layered elastic solution from Chinnery & Jovanovich (1972), we evaluate the solution for the viscoelastic problem in our supplementary IPython notebook. We find the initial viscoelastic response to a unit of slip to be

$$\frac{\partial}{\partial t}u(x,t)\big|_{t=0} = \frac{\mu}{2\eta_3}W(1,1) + \frac{\mu}{2\eta_2}(W(0,1) - W(1,1)) - \frac{\mu}{2\eta_1}W(0,1), \tag{12}$$

where

$$W(n,m) = \frac{1}{\pi}\left(\tan^{-1}\left(\frac{2nH_2 + 2mH_1 + D}{x}\right) - \tan^{-1}\left(\frac{2nH_2 + 2mH_1 - D}{x}\right)\right), \quad (13)$$

η_1, η_2, and η_3 are the viscosities of the top, middle, and bottom layers, respectively, and H_1 and H_2 are the thicknesses of the top and middle layers, respectively. We see that eq. (12) is once again linear with respect to the fluidity in each of the three layers. We can approximate early postseismic deformation resulting from slip described by $b(t)$ as

$$u(x,t) \approx b(t)\frac{1}{2}W(0,0) + \int_0^t b(\theta)\left(\frac{\mu}{2\eta_3}W(1,1) + \frac{\mu}{2\eta_2}(W(0,1) - W(1,1)) - \frac{\mu}{2\eta_1}W(0,1)\right)d\theta. \quad (14)$$

We can see that eq. (14) reduces to eq. (11) when $\eta_3 = \eta_2$.

At this point we posit that a similar approximation can be made for an arbitrarily layered lithosphere. In Appendix B we use eq. (12) to find an initial viscoelastic response kernel. We then integrate that kernel over the depth of the lithosphere to find the initial viscoelastic response for an arbitrary depth dependent viscosity structure. If the lithosphere is elastic above the fault depth, D, and described by $\eta(z)$ below D then early postseismic deformation can be approximated as

$$u(x,t) \approx \frac{b(t)}{\pi}\tan^{-1}(\frac{D}{x}) + \int_o^t \int_D^\infty \frac{\mu b(\theta)}{2\pi\eta(z)}\left(\frac{2x}{x^2 + (D+2z)^2} - \frac{2x}{x^2 + (2z-D)^2}\right)dz d\theta. \quad (15)$$

Although the above equation is capable of describing surface deformation for an arbitrary depth dependent viscosity structure, it falls short of being useful as the forward solution in an inverse problem aimed at estimating lithospheric viscosity. This shortcoming is because the above equation makes the nonphysical assumption that the fault is infinitely long, in addition to the restriction of only being applicable to a vertical strike-slip fault. The assumption of infinite length would introduce first order errors, which would likely wash out the second order effect of viscosity. However, eq. (15) is useful for making estimates of the depth sensitivity of postseismic deformation.

2.2 Three-dimensional earthquake models

Motivated by our above results, we make the assertion that the initial viscoelastic response to an instantaneous unit dislocation in a three-dimensional Maxwell viscoelastic medium, which has been arbitrarily discretized into N regions, will have the form

$$\frac{\partial}{\partial t}\vec{u}(\vec{x},t)\big|_{t=0} = \sum_j^N \frac{1}{\eta_j}G_j(\vec{x}). \quad (16)$$

We denote $\vec{u}$ and $\vec{x}$ as vectors to emphasize that eq. (16) is generalized to three-dimensional problems. We use $G_j(\vec{x})$ to represent the initial rate of surface deformation at position $\vec{x}$ resulting from viscoelastic creep in region j with unit fluidity, where fluidity is zero (i.e. elastic) in all other regions.

In this sense, $G_j(\vec{x})$ can be thought of as a Green's function for the initial viscoelastic response, and thus we refer to $G_j(\vec{x})$ as the initial viscoelastic Green's functions. We verify eq. (16) numerically in Section 4.2.1 and save a theoretical justification for a later paper.

Using eq. (16), we can approximate early surface deformation in a form that is consistent with eqs. (11) and (14):

$$\vec{u}(\vec{x},t) \approx b(t)F(\vec{x}) + \sum_{j}^{N} \int_0^t \frac{b(\theta)}{\eta_j} G_j(\vec{x}) d\theta, \tag{17}$$

where $F(\vec{x})$ is the elastic Green's function, which describes the elastic deformation resulting from a dislocation. We further generalize the approximation of surface deformation in eq. (17) to allow for an arbitrary spatial distribution of slip by using linear superposition. If the elastic deformation in a viscoelastic lithosphere can be described in terms of M elastic dislocation sources, then early surface deformation resulting from both elastic dislocations and viscous creep can be approximated as

$$\vec{u}(\vec{x},t) \approx \sum_{i}^{M} b_i(t)F_i(\vec{x}) + \sum_{i}^{M}\sum_{j}^{N} \int_0^t \frac{b_i(\theta)}{\eta_j} G_{ij}(\vec{x}) d\theta. \tag{18}$$

The initial viscoelastic Green's function is dependent upon both the region it represents as well as the dislocation source inducing the viscoelastic creep in that region, hence the two indices on $G_{ij}(\vec{x})$. It is worth restating that the approximation given above does not account for the viscoelastic coupling between the regions, since in eq. (18) each region's contribution to surface deformation is independent of the viscosity elsewhere. This approximation is therefore appropriate for as long as the regions do not significantly transfer stresses between each other through viscoelastic deformation. Alternatively, since our initial viscoelastic Green's functions do not have time dependence, one could view eq. (18) as being appropriate up until surface velocities resulting from viscoelastic creep have decayed appreciably.

3 INVERSION METHOD

The approximation of postseismic deformation given by eq. (18) can be cast as an inverse problem aimed at finding the distribution of slip on a fault and an arbitrarily complicated lithosphere viscosity structure from postseismic deformation. We assume that the slip history in any one direction on each fault patch, $b_i(t)$, can be expressed as P linear terms such that

$$b_i(t) = \sum_{k}^{P} \alpha_{ik} A_k(t), \tag{19}$$

where $A_k(t)$ can be any parameterized slip function. For this paper $A_k(t)$ consists of either unit step functions describing coseismic slip on a fault patch, or ramp functions, which increase from 0 to 1 over

some time interval, that are intended to represent afterslip. The coefficient α_{ik} then represents either the amount of coseismic slip or the cumulative slip over a time interval. The approximation given by eq. (18) now becomes

$$\vec{u}(\vec{x},t) \approx \sum_{i}^{M}\sum_{k}^{P} \alpha_{ik} F_i(\vec{x}) A_k(t) + \sum_{i}^{M}\sum_{j}^{N}\sum_{k}^{P} \int_0^t \frac{\alpha_{ik}}{\eta_j} G_{ij}(\vec{x}) A_k(\theta) d\theta. \tag{20}$$

If we assume a fault geometry and the elastic properties of the lithosphere, $F_i(\vec{x})$ can be computed with finite element software or with an analytic solution, for instance using Okada (1992) or Meade (2007). Likewise, $G_{ij}(\vec{x})$ can be computed using finite element software. If the assumed geometry of the viscoelastic regions is sufficiently simple, $G_{ij}(\vec{x})$ may also be computed with semi-analytic techniques (e.g. Pollitz 1997; Fukahata & Matsu'ura 2006; Barbot & Fialko 2010).

We estimate the unknown slip parameters, α_{ik}, and unknown viscosities in each region of the lithosphere, η_j, from observations of surface deformation in a least squares sense. Let $\boldsymbol{u_{\mathbf{obs}}}$ be a vector of observed coseismic and postseismic surface displacements at various locations and points in time. Let $\boldsymbol{m}$ be a vector of all the unknown parameters α_{ik} and η_j, and let $\boldsymbol{u(m)}$ be a vector of postseismic surface displacements predicted by eq. (20). We seek to solve

$$\min \left|\left| \boldsymbol{f(m)} \right|\right|_2^2 \tag{21}$$

subject to the constraint that

$$\boldsymbol{m} \geq 0, \tag{22}$$

where

$$\boldsymbol{f(m)} = \begin{vmatrix} \boldsymbol{W}\left(\boldsymbol{u(m)} - \boldsymbol{u_{\mathbf{obs}}}\right) \\ \lambda_s \boldsymbol{L_s m} \\ \lambda_v \boldsymbol{L_v m} \end{vmatrix}. \tag{23}$$

In the above equation, $\boldsymbol{W}$ is a diagonal matrix containing the reciprocal of the data uncertainties (i.e. $\boldsymbol{W^T W} = \boldsymbol{C_d^{-1}}$ where $\boldsymbol{C_d}$ is the data covariance matrix), and $\boldsymbol{L_s}$ and $\boldsymbol{L_v}$ are regularization matrices.

We impose a non-negativity constraint on $\boldsymbol{m}$ which ensures that inferred slip is in one predominant direction and that viscosities are positive. Specifically, the rake of the inferred slip on each fault patch is constrained to be within a 90° window defined by the rakes of chosen orthogonal basis slip directions. For instance, the basis slip directions could be chosen such that only slip rakes within 45° of pure strike-slip, normal, or thrust are permissible.

Because this inverse problem inevitably has non-unique solutions for $\boldsymbol{m}$, we put additional constraints on the inferred slip and inferred viscosity with the matrices $\boldsymbol{L_s}$ and $\boldsymbol{L_v}$, respectively. In our following synthetic test, we constrain the solution by minimizing the Laplacian of the spatial distribution of fault slip and lithospheric viscosity by letting $\boldsymbol{L_s}$ and $\boldsymbol{L_v}$ be umbrella operators (Desbrun et al.

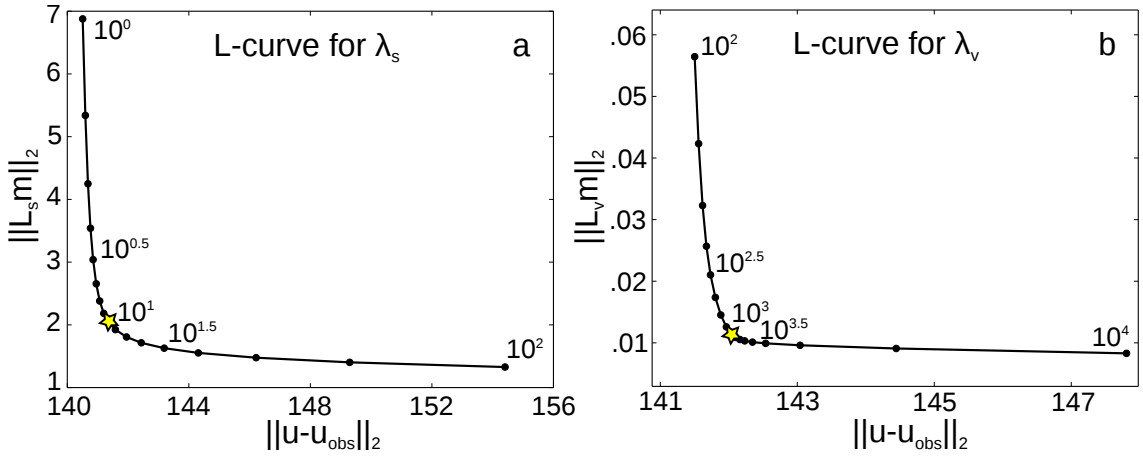

Figure 2. L-curves used to select the penalty parameters. Panel (a) shows the trade-off between slip smoothness and data misfit while varying λ_s and keeping λ_v fixed at zero. Panel (b) shows the trade off between smoothness of inferred viscosity and misfit while varying λ_v and keeping λ_s fixed at the value chosen from Panel (a). Stars indicate our chosen penalty parameters.

1999). The parameters λ_v and λ_s in eq. (23) control how much we enforce the smoothness constraint. In our synthetic test, we choose these parameters using L-curves, which describe the trade off between the model smoothness and data misfit. We first set $\lambda_v = 0$ and then use an L-curve to pick λ_s. We then fix λ_s at our chosen value and use another L-curve to pick λ_v. We explored using cross-validation to choose our model parameters, but we found that the optimal pair of penalty parameters picked through cross-validation tended to significantly degrade our fit to near-field sites.

We find $\boldsymbol{m}$ that satisfies the above conditions using the Gauss-Newton method (e.g. Aster et al. 2013). The best fit model parameters are found by making an initial guess for the solution and then iteratively solving

$$\boldsymbol{J}(\boldsymbol{m}^k)\boldsymbol{m}^{k+1} = -\boldsymbol{f}(\boldsymbol{m}^k) + \boldsymbol{J}(\boldsymbol{m}^k)\boldsymbol{m}^k \tag{24}$$

for $\boldsymbol{m}^{k+1}$, where $\boldsymbol{J}(\boldsymbol{m}^k)$ is the Jacobian of $\boldsymbol{f}(\boldsymbol{m})$ with respect to $\boldsymbol{m}$ evaluated at $\boldsymbol{m}^{\boldsymbol{k}}$. We impose the non-negativity constraint on $\boldsymbol{m}$ by solving eq. (24) with a non-negative least squares algorithm (Lawson & Hanson 1995). In a nonlinear least squares algorithm, computing the Jacobian can often be the largest computational burden when an analytic solution for the Jacobian is not available. By linearizing the viscoelastic response in early postseismic deformation with respect to $1/\eta_j$, we have made our forward problem, eq. (20), sufficiently simple that evaluating its Jacobian for a given $\mathbf{m}$ only requires a few computationally inexpensive matrix operations. Consequently, our nonlinear least squares algorithm converges to a solution for $\boldsymbol{m}$ in a matter of seconds on a desktop computer. The main computational burden is in computing $F_i(x)$ and $G_{ij}(x)$ which only needs to be done once for a given fault and lithosphere geometry.

4 SYNTHETIC TEST

We demonstrate with two synthetic tests that our inverse method is capable of recovering fault slip and an effective lithospheric viscosity from postseismic deformation. We use the finite element software, PyLith (Aagard et al. 2013), to compute the surface deformation resulting from a specified amount of slip on a fault in a lithosphere with either Maxwell or Burgers viscoelasticity. We invert this synthetic surface deformation using the method described above to recover the imposed model parameters. The synthetic tests also serve to demonstrate that eqs. (16) and (18) are indeed valid for three dimensional earthquake models.

Our synthetic models consist of a 50 km long by 20 km wide strike-slip fault, striking to the north and dipping 60° to the east (Fig. 5). At $t = 0$ we impose 6.5×10^{19} N m of surface rupturing, right-lateral coseismic slip with a distribution shown in Fig. 3. After the coseismic slip, we impose 2 years of afterslip just below the coseismic rupture zone. The spatial distribution of afterslip on the fault remains constant throughout the 2 years but the rate of afterslip decreases by a factor of 2 every 0.5 years. The cumulative moment of afterslip over the first year is about 1.6×10^{19} N m, while the cumulative moment of afterslip over the second year is 4.0×10^{18} N m. We do not impose any fault slip beyond $t = 2$ years.

We compute surface displacements at 50 randomly chosen observation points within a 400 km square centered about the fault (Fig. 5), which is intended to roughly correspond with the density of GPS station at a well instrumented plate boundary. Displacements are computed at 0.05 year intervals up until $t = 10$ years. We add temporally correlated noise to the computed displacements through time, consistent with what one would expect from GPS observations. The standard deviation of northing and easting displacements is 1 mm, and the standard deviation of the vertical displacements is 2.5 mm. We add temporal covariance with an exponential noise model that has a characteristic timescale of 0.25 years, which is intended to simulate seasonal processes that are typically present in GPS time series.

4.1 Green's functions

We invert the synthetic surface displacements for fault slip on a 4 km by 4 km discretization of the planar fault. We estimate a constant viscosity in 10 km thick horizontal layers from the surface down to 70 km depth and for a lower substrate. We compute the elastic Green's functions, $F_i(\vec{x})$, and initial viscoelastic Green's functions, $G_{ij}(\vec{x})$, numerically using PyLith. The elastic Green's functions are the initial surface displacements resulting from 1 m of imposed slip on fault patch i. For each fault patch, we use basis slip directions with rake 45° up-dip and 45° down-dip of pure right-lateral slip. These slip basis directions restrict all inferred slip to have rakes within 45° of right-lateral. We find the initial viscoelastic Green's functions, $G_{ij}(\vec{x})$, by computing the initial rate of surface deformation

due to 1 m of slip on fault patch i in a model that is elastic everywhere except in region j, which is assigned a unit fluidity. In the interests of numerical stability we used 10^{-18} Pa^{-1} s^{-1} as our unit of fluidity. We emphasize that the amount we perturb the fluidity in region j will have no influence on our computation of $G_{ij}(x)$ because the initial rate of deformation computed with Pylith will be proportional to $G_{ij}(x)$ times our fluidity perturbation.

We define the basis slip functions, $A_k(t)$, as a Heaviside function centered at $t = 0$ and twenty ramp functions which describe 1 m of cumulative slip over the time intervals $t = (0, 0.5), (0.5, 1.0), \ldots,$ and $(9.5, 10.0)$ years. We note that the synthetic model does not have any fault slip from $t = 2$ to 10 years and the postseismic deformation over that interval is resulting purely from viscoelastic creep.

4.2 Synthetic model with Maxwell viscoelasticity

The lithosphere in our first synthetic model is Maxwell viscoelastic with homogeneous Lamé parameters $\lambda = 32$ GPa and $\mu = 32$ GPa. The viscosity in the lithosphere decays from 10^{21} Pa s ($\tau \approx 1,000$ years) at the surface to 10^{19} Pa s ($\tau \approx 10$ years) at 75 km depth (Fig. 4). For the timescales of this synthetic test, the uppermost lithosphere is effectively elastic.

We use the penalty parameters chosen in Fig. 2 and our recovered model of slip on the fault is shown in Fig. 3. We use 100 iterations of bootstrapping to assess how sensitive our recovered model is to the imposed data noise. The standard deviation of coseismic slip and cumulative afterslip over the indicated interval is shown in the right column of Fig. 3. The spatial distribution and direction of inferred coseismic slip are a good match to the synthetic coseismic slip. The distribution of afterslip was decently recovered but not as well as the coseismic slip was recovered. Inferred afterslip over the first year is smoother than the true slip due to the regularization, although there is a high concentration of slip on the northern portion of the fault which is consistent with the synthetic model. We attribute the better resolved northern portion of the fault to a proximal surface observation point. There are a few artifacts in the distribution of inferred afterslip from $t = 1$ to 2 years which are not present in the synthetic model, such as slip on the deepest portion of the fault. Our inability to recover the details of the imposed afterslip as well as the coseismic slip could be because the data noise is obscuring some of the postseismic signal (Fig. 5b and 5c compared to Fig. 5a) and causing higher variability in inferred slip models. Nevertheless, the inferred moment of both coseismic slip and afterslip, which is proportional to slip integrated over the fault plane, is within 10% of the moment in the synthetic model. Although the spatial distribution of inferred slip may be more difficult to recover, the slip moment seems to be consistently recovered.

The inferred slip over the last time interval, $t = 2$ to 10 years, is also consistent with the synthetic model. The moment of slip over this interval is 8.1×10^{17} N m, which is two orders of magnitude

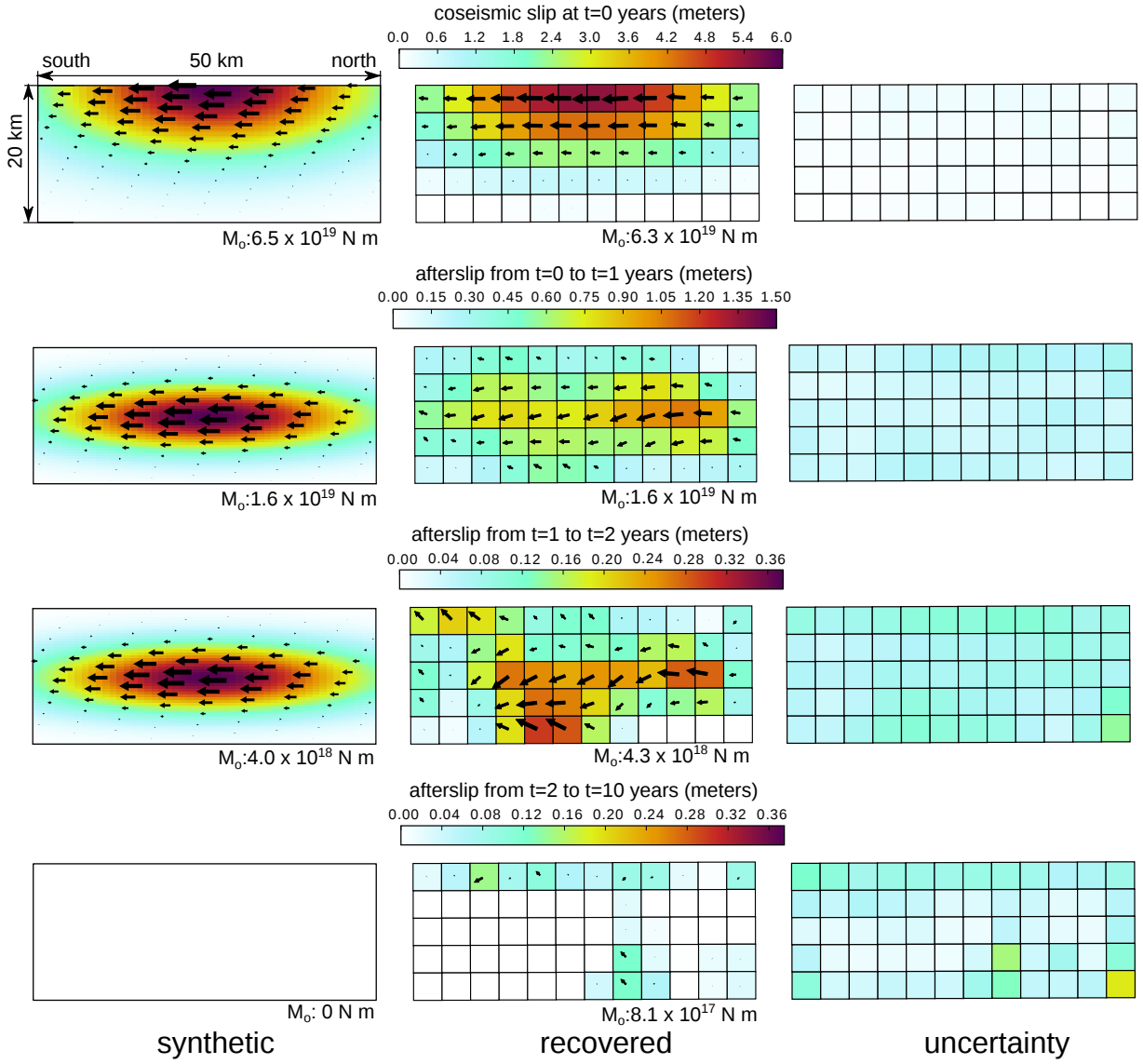

Figure 3. Slip distribution imposed in both synthetic models (left), slip recovered for the synthetic model with Maxwell viscoelasticity (middle), and uncertainty in the recovered slip magnitude (right). Colors indicate magnitude of slip and arrows indicate direction of slip (arrows pointing right indicate left-lateral and up is thrust). The panels showing afterslip display cumulative slip over the specified time interval. The slip uncertainties are the standard deviation of inferred slip magnitude during the specified period, which were derived from 100 iterations of bootstrapping.

smaller than the moment for the coseismic slip in the synthetic model and is accounting for, at most, a few mm's of surface displacement from $t = 2$ to 10 years, which is on order of the data uncertainty. We can further dismiss inferred afterslip during this period as being negligibly small because the magnitude of inferred slip is on order of the the uncertainty inferred from bootstrapping (Fig. 3). The

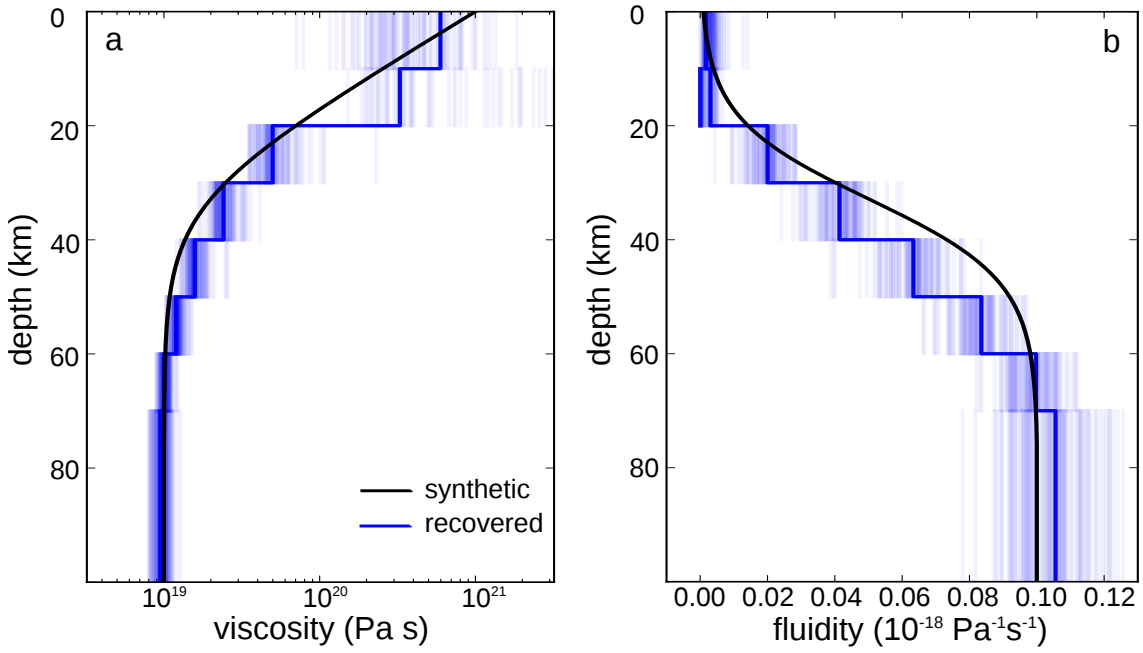

Figure 4. Synthetic and recovered lithospheric viscosities (left) and associated fluidities (right). Semi-transparent lines are recovered models found through bootstrapping and indicate the degree of uncertainty on the inferred viscosity structure.

majority of surface deformation during this time interval (Fig. 5d) is therefore being properly attributed to viscoelastic relaxation in the inversion results.

The inferred viscosities in each of the eight layers are shown in Fig. 4(a). The recovered viscosities correspond well with the synthetic model. The uncertainties of the recovered viscosities are inferred using bootstrapping and we find that the strongest layers near the surface, despite being close to the earthquake source, have the highest uncertainties. However, viscosities greater than 10^{20} Pa s are effectively elastic on the timescales of this synthetic test and so a wide range of high viscosities for the upper layers would just as adequately be able to describe the synthetic surface displacements. When looking at inferred values of fluidity (Fig. 4b), we see that the uncertainties are lowest at the surface and increase with depth, as is perhaps more intuitive.

Viscoelastic relaxation immediately below the fault and afterslip on the fault would have similar surface manifestations, and thus it is reasonable to explore the trade-off between these processes. We use the collection of models obtained through bootstrapping and compute the correlation coefficient between the estimates of cumulative afterslip moment over 10 years and the inferred fluidity for select layers. Not surprisingly, the correlation coefficient is -0.16, and -0.25 in the layer from 10 to 20 km depth and 20 to 30 km depth, respectively, which means that higher estimates of fluidities in those layers tend to be compensated by lower estimates of slip on the fault. Interestingly, there is a posi-

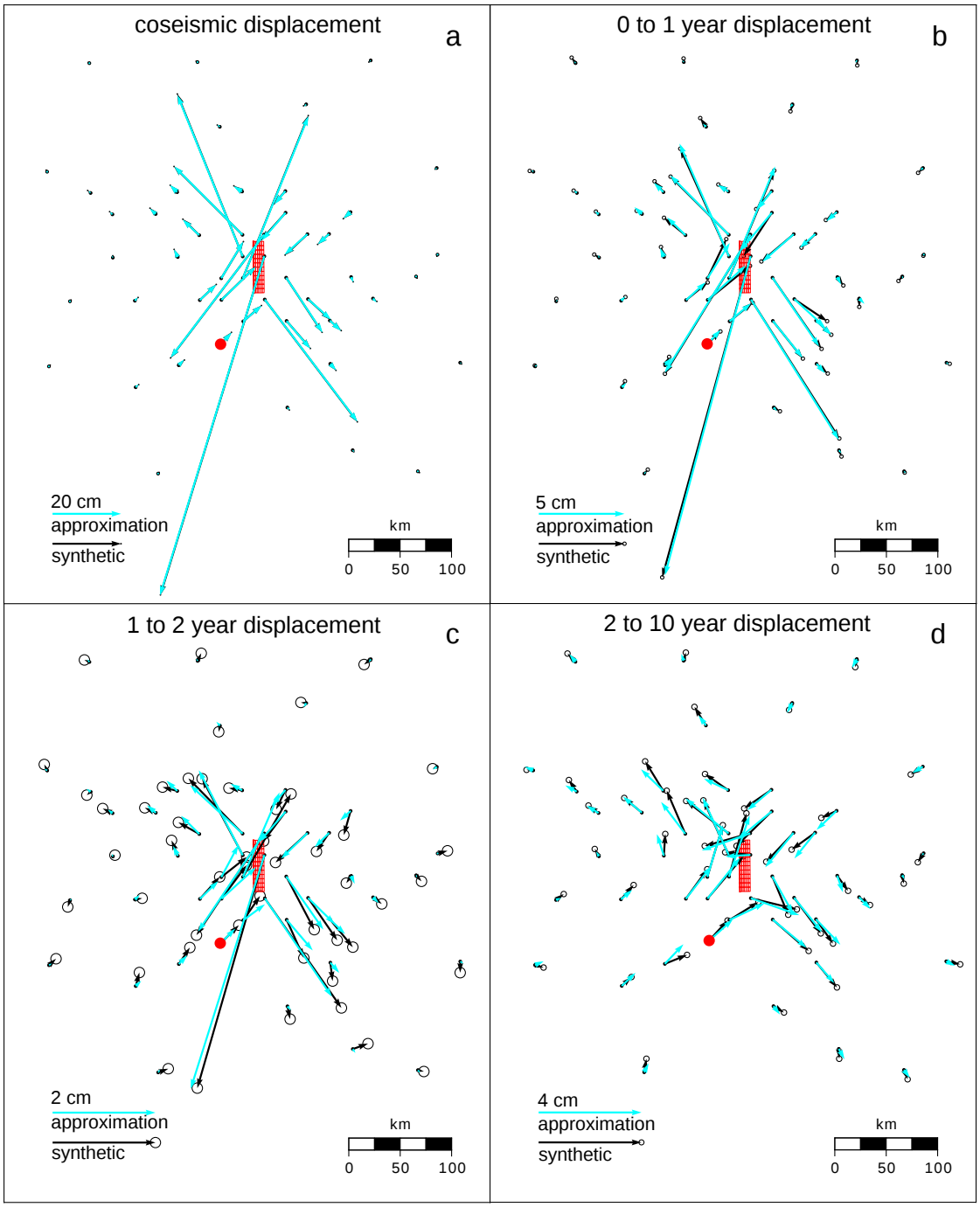

Figure 5. Synthetic surface displacements (black) and best fitting surface displacements using eq. (20) (cyan). Vertical displacements are used in the inversion but are not shown here. Panel (a) shows coseismic displacements and the remaining panels show the cumulative displacements over the indicated time intervals. Ellipses indicate 1 standard deviation uncertainty in the synthetic data. Red dot indicates the position of the time series shown in Fig. 6 and Fig. 9. The surface projection of the discretized synthetic fault is depicted in red.

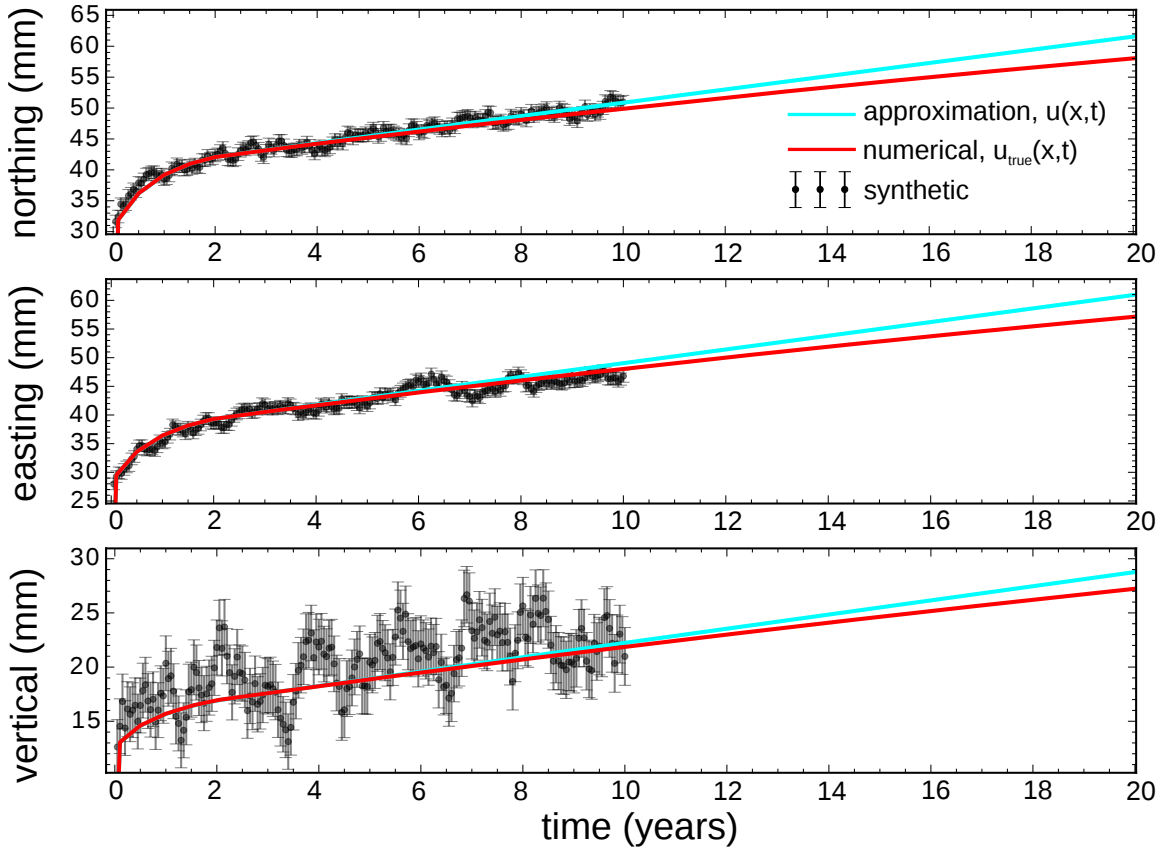

Figure 6. Displacement time series for the position shown in Fig. 5 (black), best fitting surface displacements using the approximation from eq. (20) (cyan) and surface displacements computed with PyLith using the inferred slip distribution and viscosity structure (red). Coseismic displacements at $t = 0$ are not shown.

tive correlation of 0.38 between cumulative afterslip moment and the fluidity in the uppermost layer containing the fault. The positive correlation is because deformation resulting from viscoelastic relaxation in the uppermost layer containing the fault tends to be in the opposite direction as deformation resulting from fault slip. This means that a high fluidity in the uppermost layer will tend to produce deformation that is balanced out by higher amounts of slip. It is conceivable that such a correlation could lead to unrealistic inferences of viscosity in the near surface and it may be necessary to assume that viscous regions containing a fault are elastic. There is no significant correlation between afterslip and fluidity in layers below 30 km depth.

4.2.1 Validation

The fact that our recovered fault slip and lithospheric viscosity are in good agreement with the synthetic model suggests that the approximation given by eq. (20) is accurate over the 10 years of synthetic data. We further assess the accuracy of eq. (20) by running a forward model with PyLith where

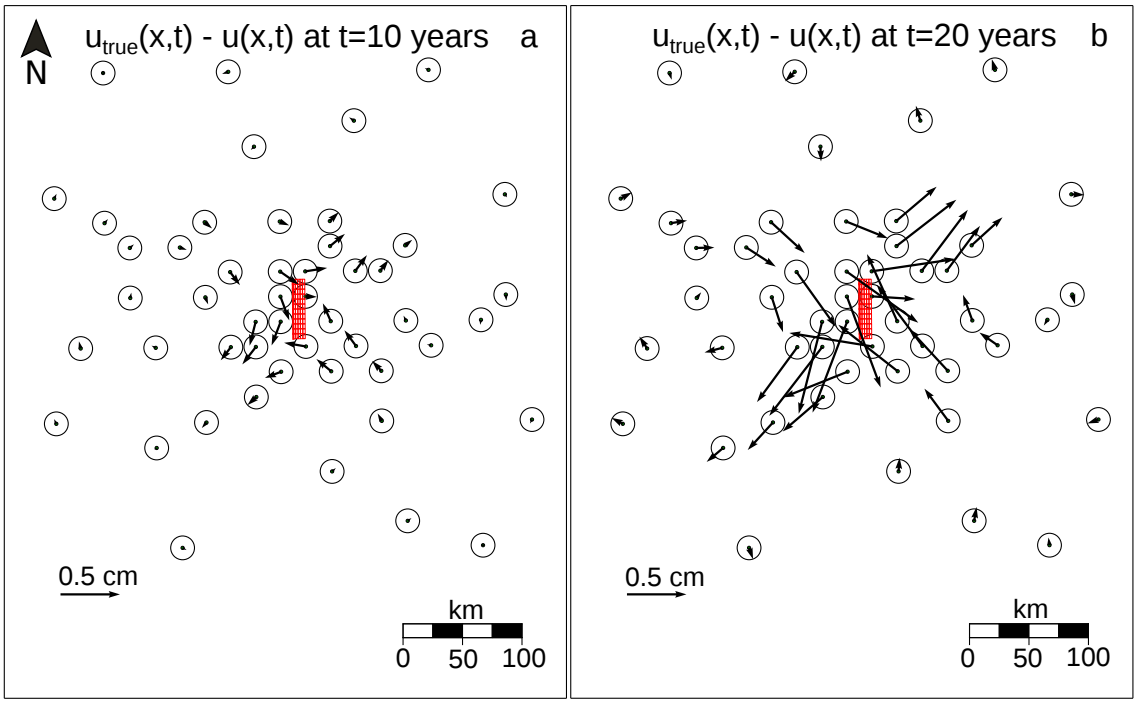

Figure 7. Approximation error at $t = 10$ years and $t = 20$ years. Circles with 1 mm radius are centered at each station to compare the accuracy of $\vec{u}(\vec{x}, t)$ to the noise in the synthetic data.

the imposed fault slip and lithospheric viscosity are those estimated from the synthetic data. We then compare the displacements from the numerically computed forward model with the displacements predicted by eq. (20). We refer to the numerically computed displacements as $\vec{u}_{\rm true}(\vec{x}, t)$ and the displacements predicted by the approximation as $\vec{u}(\vec{x}, t)$ (Fig. 6). We refer to the difference between $\vec{u}_{\rm true}(\vec{x}, t)$ and $\vec{u}(\vec{x}, t)$ as the approximation error (Fig. 7). At $t = 10$ years the approximation error is on order of a few mm's for each location, which is the magnitude of the data uncertainty. Additionally, the approximation error is small compared to the cm's of deformation resulting from viscoelastic relaxation, indicating that eq. (20) is indeed a fair approximation up to $t = 10$ years. At $t = 20$ years the approximation error is about one cm in magnitude for near field sites, indicating that the approximation has broken down in the near field by this time, while the error is still on order of a few mm's for the far field sites. The faster divergence for the near field sites is consistent with the comparison we made between the approximate and true displacements for a two-dimensional, two layered earthquake model in Section 2.1.1 (Fig. 1).

The accuracy of eq. (20) is also demonstrated in Fig. 6, which shows $\vec{u}(\vec{x}, t)$ and $\vec{u}_{\rm true}(\vec{x}, t)$ at a sample site near the fault. The numerical solution asymptotically approaches the rate of deformation predicted by eq. (20) as time goes to zero, demonstrating that eq. (16) accurately describes the initial viscoelastic response. Additionally, the magnitude of the difference between $\vec{u}(\vec{x}, t)$ and $\vec{u}_{\rm true}(\vec{x}, t)$ is

smaller than the uncertainty of our synthetic data throughout the time series, indicating that eq. (20) is appropriate for this synthetic test. For this site and other near field sites, the approximation starts to break down at about $t = 10$ years. The lowest relaxation time in our synthetic lithosphere is also about 10 years and so the duration over which eq. (20) is accurate is longer than what we found in our analysis for a two-dimensional, two layered earthquake model in Section 2.1.1.

4.3 Synthetic model with Burgers viscoelasticity

In the above synthetic example, we conveniently picked the length of our displacement time series to correspond with the shortest relaxation time in the lithosphere. If the length of the time series is significantly shorter than the relaxation time of the lithosphere, then eq. (20) would be an appropriate approximation and fault slip would be accurately recovered, although there would not be a significant amount of deformation resulting from viscoelastic relaxation and so inferences of viscosity would have high uncertainty. When the length of the time series is significantly longer than the shortest relaxation time of the lithosphere then the approximation would not be accurate and we would see a notable misfit in our best fitting prediction of the data. Here we use another synthetic test to demonstrate an iterative approach to finding the optimal time series duration. We also use this synthetic test to demonstrate how fluidities inferred using our inverse method can be used to constrain the viscous properties of a non-Maxwell viscoelastic lithosphere.

We consider a synthetic model with the same fault geometry and prescribed slip as the synthetic model described in Section 4.2, but the lithosphere now has a Burgers rheology. A Burgers rheology can be modeled schematically as a Maxwell spring-dashpot system connected in series with a Kelvin spring-dashpot system. There are five rheologic parameters needed to describe a Burgers rheology, the first Lamé parameter, λ, shear moduli of the Maxwell and Kelvin elements, μ_m and μ_k, and the viscosities of the Maxwell and Kelvin elements, η_m and η_k. In this synthetic test, we set $\mu_m = \lambda = 32$ GPa and η_m equal to the viscosity structure from the synthetic model in Section 4.2. We also set $\mu_k = \mu_m$ and $\eta_k = 0.1\eta_m$ so the lowest kelvin relaxation time (η_k/μ_k) in our synthetic model is 1 year (Fig. 8).

We use the same $F_i(\vec{x})$, $G_{ij}(\vec{x})$, and $A_k(t)$, described in Section 4.1 and estimate an effective Maxwell viscosity by using 0.5, 2.0 and 5.0 years of synthetic data. Our inverse method allows us to estimate a single value of viscosity for each discretized region of the lithosphere and so we are unable to recover both η_k and η_m. Instead, our method allows us to estimate an effective viscosity for a Burgers viscoelastic lithosphere during the early postseismic period. We demonstrate in our supplementary IPython notebook that when assuming μ_m is equal to the shear modulus used to construct $F_i(\vec{x})$ and

$G_{ij}(\vec{x})$ then the effective fluidity inferred using our method, $1/\eta$, is equivalent to

$$\frac{1}{\eta} = \left(\frac{1}{\eta_k} + \frac{1}{\eta_m} \right). \tag{25}$$

The recovered viscosities for each time series duration are shown in Fig. 8 and we show the moment of inferred afterslip as a function of time in Fig. 9. The synthetic and predicted displacement time series at the observation point indicated in Fig. 5 are shown in Fig. 10. We are able to accurately predict the synthetic displacements (red line in Fig. 10) and recover the fluidities expected following eq. (25) when using a 0.5 year time series. The relatively few number of observations constraining the fluidity inferences leads to large uncertainties as indicated by the distribution of bootstrapped models. When we use 2 years of displacements, exceeding the minimum Kelvin relaxation time in the synthetic model, the best fitting predicted displacements are still a good fit to the synthetic data (green line), but it is difficult to discern whether some of the systematic misfit is due to the inability of eq. (20) to describe the transient displacement or because of the temporal correlation of our added noise. The inferences of fluidity when using 2 years of displacement are consistently off by a factor of 0.5. The underestimation of fluidity is then compensated by a slight overestimation of cumulative fault slip (Fig. 9). Although the estimated fluidities are incorrect, the relative strength of the different layers is well recovered. When using 5 years of synthetic deformation, the depth dependence of fluidity no longer resembles the true depth dependence and the inferred moment of afterslip is appreciably higher than what was imposed in the synthetic model. Even though additional afterslip is describing some of the transient viscoelastic deformation, there is still a systematic misfit in the best fitting prediction to the 5 year time series (Fig. 10) indicating that eq. (20) is not valid for that duration of time. The length of the time series used for our inverse method should be just long enough so that the best fitting predictions to the data do not have any systematic misfit. It is difficult to distinguish by the fit to the data whether the model recovered using a 0.5 year time series or a 2 year time series is a better estimate of the true model, although one can easily run a forward calculation for each of the recovered models to see how well they predict the later deformation.

5 DISCUSSION

A fundamental assumption in our method for estimating slip and viscosity from postseismic deformation is that the timescale of relaxation in the weakest part of the lithosphere is at least as long as the timescales over which postseismic deformation is observed. This assumption allows us to approximate the surface expression of viscous creep as a linear system with respect to lithospheric fluidity, which greatly facilitates and expedites the inverse problem. Since the relaxation times in a given region are

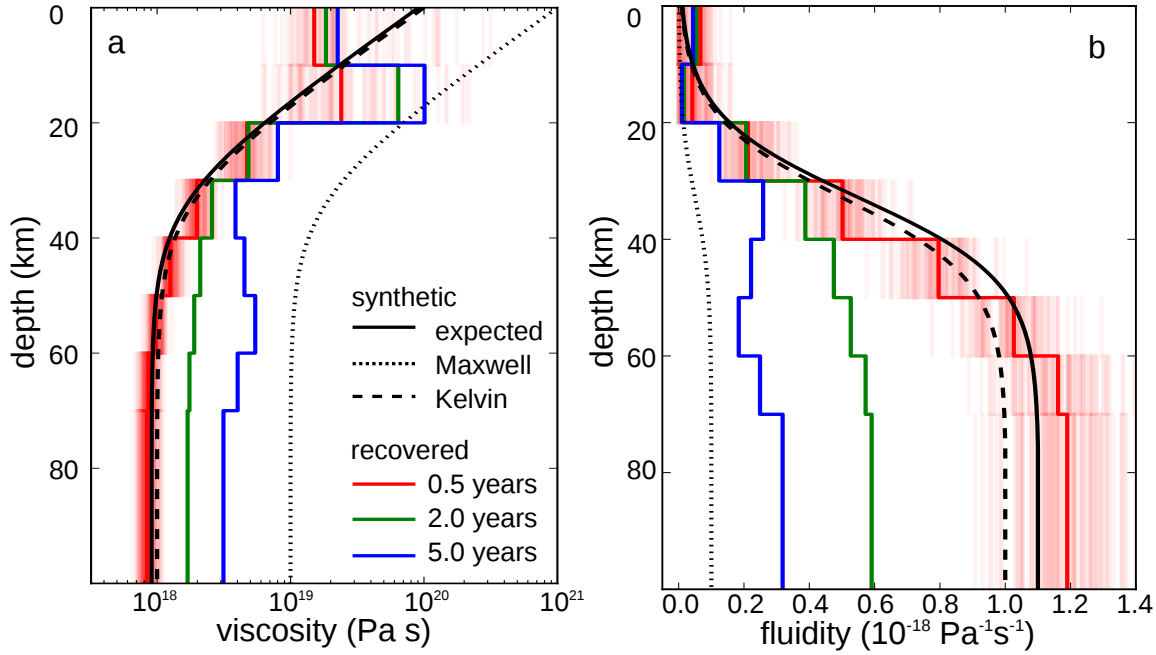

Figure 8. Synthetic and recovered lithospheric viscosities (left) and fluidities (right) for the synthetic model with a Burgers rheology. Dotted and dashed lines show the Maxwell and Kelvin viscosity in the synthetic model, respectively. The solid black line indicates the effective viscosity from eq. (25). The red, green, and blue lines show the inferred viscosities and fluidities when inverting a 0.5, 2.0, and 5.0 year long time series, respectively. The light red lines are the bootstrapped fluidities and viscosities inferred using the 0.5 year time series.

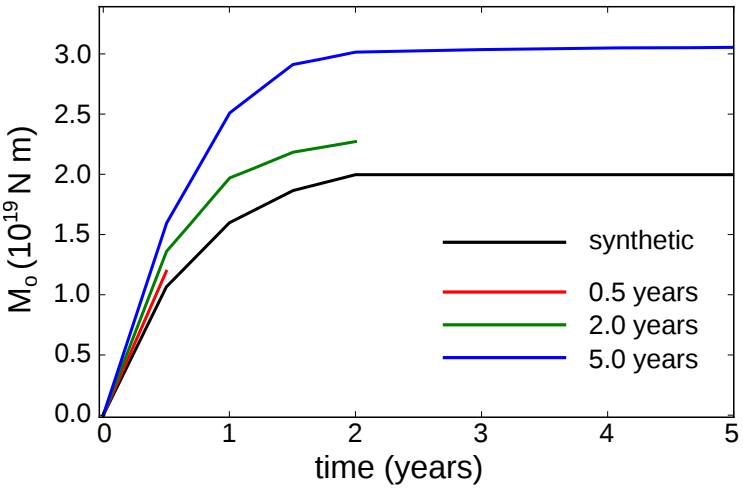

Figure 9. Afterslip moment over time for the synthetic model (black) and the inferred afterslip moment when inverting 0.5, 2.0, and 5.0 years of displacements (red, green, and blue)

.

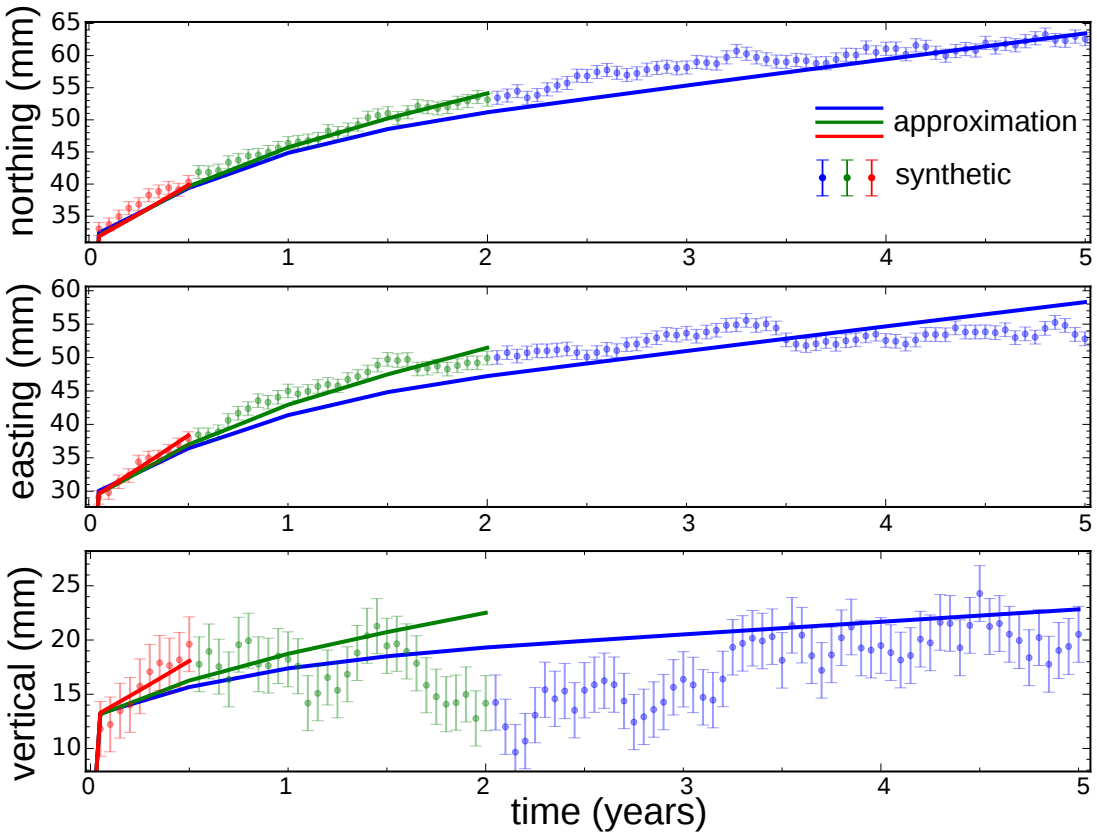

Figure 10. Synthetic and predicted displacement time series with length 0.5, 2.0, and 5.0 years. The time series shown is for the observation point indicated in Fig 5.

generally not well known *a priori*, one must use an iterative approach as described in Section 4.3 to determine the appropriate length of the time series used in the inversion.

We can look at previous studies to gauge the duration over which our approximation would be accurate. Surface deformation following large ($\geq M_w = 7$) earthquakes often is characterized by transient and rapid postseismic deformation in the first year after and earthquake followed by steady deformation in later years (e.g. Savage & Svarc 1997; Savage et al. 2005; Ergintav et al. 2009). Several studies have attributed rapid early transient deformation following an earthquake to afterslip, while describing the later steady deformation with viscous relaxation in a Maxwell viscoelastic lower crust or upper mantle (e.g. Perfettini et al. 2005; Johnson et al. 2009; Hearn et al. 2009; Freed et al. 2006a; Rollins et al. 2015). These studies have found that lithospheric relaxation times no shorter than years or decades are needed to describe postseismic deformation. Indeed, Perfettini et al. (2005) describes the trend in two years of postseismic deformation following the 2001 $M_w = 8.4$ Peru earthquake by assuming that the lithospheric viscosity was sufficiently high that the rate of deformation from viscoelastic creep could be considered constant, which is the assumption that

we make in formulating eq. (18). If transient postseismic deformation can be attributed to fault slip followed by steady viscoelastic creep, then eq. (18) should be able to describe displacements on the timescale of years or decades after an earthquake.

Several studies have used rheologies containing a transient phase of deformation to explain the early postseismic deformation. For example, Pollitz (2003, 2005) invoked a Burgers rheology upper mantle to explain surface displacements following the 2002 $M_w = 7.9$ Denali earthquake and the 1999 $M_w = 7.1$ Hector Mine earthquake. In both cases the best fitting transient relaxation time was on the order of a month and the best fitting steady-state relaxation time was on the order of years. Postseismic deformation following the Denali earthquake was also successfully modeled by Freed et al. (2006b) with a power-law rheology in the upper mantle, consistent with laboratory studies (e.g. Kirby and Kronenberg 1987). The power-law rheology was able to reproduce the observed transient surface deformation because the high stresses in the earthquake decreased the effective viscosity of the upper mantle to $\sim 10^{17}$ Pa s resulting in fast surface deformation. As stresses from the earthquake relaxed, the effective viscosity increased and the predicted surface deformation became steadier. Based on the success of Pollitz (2003, 2005) and Freed et al. (2006b), one may dismiss our method as being unrealistic because we assume that the lithosphere is Maxwell viscoelastic. However, our method does not necessarily preclude the possibility of a Burgers rheology, as demonstrated in Section 4.3, or a stress-nonlinear viscosity. As long as stresses in the lithosphere remain roughly equal to the the stresses transferred elastically through fault slip, then a viscosity structure inferred using our method could be interpreted as the effective viscosity in a transient viscoelastic or power-law rheology. One could also use eq. (25) to constrain the rheologic properties for a Burgers rheology. If the commonly observed early transient postseismic deformation truly is the result of viscous relaxation in the lithosphere rather than afterslip, then the results from Pollitz (2003, 2005) and Freed et al. (2006b) suggest that the time interval over which eq. (18) is appropriate is on order of a month after an earthquake. In such case, our method can be used to get an initial estimate of lithospheric viscosity, while unused portion of the displacement time series could be incorporated in a gradient based nonlinear inverse method where the forward problem is computed numerically rather than with eq. (18).

Postseismic transient deformation could also be the result of creep in a weak ductile shear zone which is embedded in a stronger viscoelastic lithosphere (e.g. Hetland & Zhang 2014). Sufficiently localized creep in a shear zone can be modeled as slip on a down-dip extension of the ruptured fault (e.g. Hearn et al. 2002; Kenner & Segall 2003; Johnson & Segall 2004) because the two processes are kinematically indistinguishable. Likewise, Freed et al. (2006b) noted that deep fault slip could serve as a proxy for distributed viscous relaxation in a weak lower crust when only considering horizontal

displacements. The applicability of our method should therefore be unaffected by localized viscous deformation with the understanding that inferences of fault slip could be absorbing that deformation.

6 CONCLUSION

We present a method to invert coseismic and postseismic deformation to simultaneously estimate a time dependent distribution of fault slip and an arbitrarily discretized viscosity structure of the lithosphere. We take advantage of an approximation for early postseismic deformation resulting from fault slip and viscoelastic relaxation. This approximation is computationally efficient which allows us to rapidly search a high dimensional model space and make higher resolution estimates of effective lithospheric viscosity than what can feasibly be done with the commonly used grid search methods. Our method is applicable for as long as this approximation is appropriate, that is, for as long as stresses resulting from coseismic slip and afterslip have not significantly decayed due to viscoelastic relaxation. Based on inferences of lithospheric viscosity from other studies, we estimate that our method could be used for postseismic deformation ranging from months to years after an earthquake. Despite our methods application to a limited portion of the postseismic period, we demonstrate that our method is capable of robustly recovering the mechanisms driving postseismic deformation.

APPENDIX A: INVERSE LAPLACE TRANSFORM THROUGH SERIES EXPANSION

Let $f(t)$ be analytic at $t = 0$ and let there be a real valued M, and C such that

$$\left|f^{(n)}(t)\right| < Ce^{Mt} \quad \forall t \geq 0 \text{ and } \forall n \in \{0, 1, 2, \dots\}, \tag{A.1}$$

where $f^{(n)}(t)$ denotes the n^{th} derivative of $f(t)$. We define the Laplace transform of $f(t)$ as

$$\mathcal{L}[f(t)] := \hat{f}(s) := \int_0^\infty f(t)e^{-st}dt \tag{A.2}$$

and we restrict our attention to $s \in \mathbb{R}$. The constraints on $f^{(n)}(t)$ from eq. (A.1) ensure that

$$\lim_{s\to\infty} \mathcal{L}[f^{(n)}(t)] = 0. \tag{A.3}$$

It can be shown using integration by parts that

$$\mathcal{L}[f^{(n)}(t)] = s^n \hat{f}(s) - \sum_{m=1}^{n} s^{m-1} f^{(n-m)}(0) \quad \forall s > M. \tag{A.4}$$

Substituting eq. (A.4) into eq. (A.3) and then rearranging the terms gives us a recursive formula for $f^{(n)}(0)$ in terms of $\hat{f}(s)$:

$$f^{(n)}(0) = \lim_{s\to\infty} s^{n+1} \hat{f}(s) - \sum_{m=1}^{n} s^m f^{(n-m)}(0), \tag{A.5}$$

where the base case, $n = 0$, is the initial value theorem:

$$f(0) = \lim_{s\to\infty} s\hat{f}(s). \tag{A.6}$$

Since we request $f(t)$ to be analytic at $t = 0$, we can construct a Taylor series expansion of $f(t)$ such that

$$f(t) = \sum_{n=0}^{\infty} \frac{f^{(n)}(0)}{n!} t^n \tag{A.7}$$

for all values of t within some neighborhood of $t = 0$. We find the inverse Laplace transform of $\hat{f}(s)$ by combining eq. (A.7) with eqs. (A.5) and (A.6) so that $f(t)$ is expressed in terms of $\hat{f}(s)$.

APPENDIX B: POSTSEISMIC APPROXIMATION FOR A TWO-DIMENSIONAL EARTHQUAKE MODEL WITH A DEPTH DEPENDENT VISCOSITY

We seek to find an approximation for early postseismic deformation in a two-dimensional, strike-slip earthquake model with an arbitrary depth-dependent viscosity below the fault locking depth, D. We first find the initial rate of surface deformation following a unit of slip in a lithosphere that is elastic except for a viscoelastic layer which is at depth z and with thickness Δz. This is found by making the substitutions $H_1 \to z$, $H_2 \to \Delta z$, $\eta_1 \to \infty$, $\eta_3 \to \infty$, and $\eta_2 \to \eta$ in eq. (12), which gives us

$$\frac{\partial}{\partial t} u_1(x,t)\big|_{t=0} = \frac{1}{\eta}(W(z+\Delta z) - W(z)), \tag{B.1}$$

where

$$W(z) = \frac{\mu}{2\pi}\left(\tan^{-1}\left(\frac{2z-D}{x}\right) - \tan^{-1}\left(\frac{2z+D}{x}\right)\right). \tag{B.2}$$

From eq. (16) we know that the initial rate of surface deformation for a lithosphere composed of N discrete layers, each with viscosity η_i, at depth z_i, and having thickness Δz, is then

$$\frac{\partial}{\partial t} u_N(x,t)\big|_{t=0} = \sum_{i}^{N} \frac{1}{\eta_i}(W(z_i+\Delta z) - W(z_i)). \tag{B.3}$$

The initial rate of surface deformation for a viscosity structure given by $\eta(z)$ is found by taking the limit as $\Delta z \to 0$ and $N \to \infty$:

$$\frac{\partial}{\partial t} u(x,t)\big|_{t=0} = \int_D^{\infty} \frac{1}{\eta(z)} \frac{\partial}{\partial z} W(z) dz \tag{B.4}$$

$$= \int_D^{\infty} \frac{\mu}{2\pi\eta(z)} \left(\frac{2x}{x^2 + (D+2z)^2} - \frac{2x}{x^2 + (2z-D)^2}\right) dz. \tag{B.5}$$

Finally, we add the elastic component of deformation and integrate eq. (B.5) with the fault slip history to obtain an approximation for early postseismic deformation:

$$u(x,t) \approx \frac{b(t)}{\pi} \tan^{-1}(\frac{D}{x}) + \int_o^t \int_D^{\infty} \frac{\mu b(\theta)}{2\pi\eta(z)} \left(\frac{2x}{x^2 + (D+2z)^2} - \frac{2x}{x^2 + (2z-D)^2}\right) dz d\theta. \tag{B.6}$$

REFERENCES

Aagaard, B.T., Knepley, M.G. & Williams, C.A., 2013. A domain decomposition approach to implementing fault slip in finite-element models of quasi-static and dynamic crustal deformation, *J. Geophys. Res. Solid Earth*, 118, doi: 10.1002/jgrb.50217.

Aster, R.C., Borchers, B., Thurber, C.H., 2013. Parameter estimation and inverse problems, *Academic Press*.

Barbot, S., Fialko, Y. & Bock, Y., 2009. Postseismic deformation due to the Mw 6.0 2004 Parkfield earthquake: Stress-driven creep on a fault with spatially variable rate-and-state friction parameters, *J. Geophys. Res. Solid Earth*, 114, 1-26. doi:10.1029/2008JB005748.

Barbot, S. & Fialko, Y., 2010. A unified continuum representation of post-seismic relaxation mechanisms: Semi-analytic models of afterslip, poroelastic rebound and viscoelastic flow, *Geophys. J. Int.*, 182, 1124-1140. doi:10.1111/j.1365-246X.2010.04678.x.

Bürgmann, R., Ergintav, S., Segall, P., Hearn, E.H., McClusky, S., Reilinger, R.E., Woith, H. & Zschau, J., 2002. Time-dependent distributed afterslip on and deep below the İzmit earthquake rupture, *Bull. Seismol. Soc. Am.*, 92, 126-137. doi:10.1785/0120000833.

Chinnery, M.A. & Jovanovich, D.B., 1972. Effect of earth layering on earthquake displacement fields, *Bull. Seismol. Soc. Am.*, 62, 1629-1639.

Desbrun, M., Meyer, M., Schröder, P. & Barr, A.H., 1999. Implicit fairing of irregular meshes using diffusion and curvature flow, *Proceedings of the 26th Annual Conference on Computer Graphics and Interactive Techniques*, 317324. doi:10.1145/311535.311576.

Ergintav, S., McClusky, S., Hearn, E., Reilinger, R., Cakmak, R., Herrring, T., Ozener, H., Lenk, O. & Tari, E., 2009. Seven years of postseismic deformation following the 1999, M = 7.4 and M = 7.2, İzmit-Düzce, Turkey earthquake sequence. *J. Geophys. Res. Solid Earth*, 114. doi:10.1029/2008JB006021.

Flügge, W., 1975. Viscoelasticity, Springer-Verlag Berlin Heidelberg.

Freed, A.M., Bürgmann, R., Calais, E., Freymueller, J. & Hreinsdóttir, S., 2006. Implications of deformation following the 2002 Denali, Alaska, earthquake for postseismic relaxation processes and lithospheric rheology. *J. Geophys. Res. Solid Earth*, 111, 1-23. doi:10.1029/2005JB003894.

Freed, A.M., Bürgmann, R., Calais, E. & Freymueller, J., 2006. Stress-dependent power-law flow in the upper mantle following the 2002 Denali, Alaska, earthquake, *Earth Planet. Sci. Lett.*, 252, 481-489. doi:10.1016/j.epsl.2006.10.011.

Freed, A.M., 2007. Afterslip (and only afterslip) following the 2004 Parkfield, California, earthquake, *Geophys. Res. Lett.*, 34, 1-5. doi:10.1029/2006GL029155.

Fukahata, Y., Matsuura, M., 2006. Quasi-static internal deformation due to a dislocation source in a multilayered elastic/viscoelastic half-space and an equivalence theorem. *Geophys. J. Int.*, 166, 418-434. doi:10.1111/j.1365-246X.2006.02921.x.

Harris, R.A. & Segall, P., 1987. Detection of a locked zone at depth on the Parkfield, California, segment of the San Andreas Fault. *J. Geophys. Res.*, 92, 7945-7962. doi:10.1029/JB092iB08p07945.

Hearn, E.H., Bürgmann, R. & Reilinger, R.E., 2002. Dynamics of İzmit earthquake postseismic de-

formation and loading of the Düzce earthquake hypocenter. *Bull. Seismol. Soc. Am.*, 92, 172-193. doi:10.1785/0120000832.

Hearn, E.H., McClusky, S., Ergintav, S. & Reilinger, R.E., 2009. İzmit earthquake postseismic deformation and dynamics of the North Anatolian Fault Zone. *J.Geophys. Res. Solid Earth*, 114, 1-21. doi:10.1029/2008JB006026.

Hetland, E.A. & Hager, B.H., 2005. Postseismic and interseismic displacements near a strike-slip fault: A two-dimensional theory for general linear viscoelastic rheologies. *J. Geophys. Res. Solid Earth*, 110, 1-21. doi:10.1029/2005JB003689.

Hetland, E.A. & Hager B.H., 2003. Postseismic relaxation across the Central Nevada Seismic Belt, *J. Geophys. Res.*, 108, 113. doi:10.1029/2002JB002257.

Hetland, E.A. & Zhang, G., 2014. Effect of shear zones on post-seismic deformation with application to the 1997 Mw 7.6 Manyi earthquake, *Geophys. J. Int.*, 198, 259-269. doi:10.1093/gji/ggu127.

Hines, T.T. & Hetland, E.A., 2013. Bias in estimates of lithosphere viscosity from interseismic deformation, *Geophys. Res. Lett.*, 40, 4260-4265. doi:10.1002/grl.50839.

Hsu, Y.-J., Simons, M., Avouac, J.-P., Galetzka, J., Sieh, K., Chlieh, M., Natawidjaja, D., Prawirodirdjo, L. & Bock, Y., 2006. Frictional Afterslip Following the 2005 Nias-Simeulue Earthquake, Sumatra, *Science*, 312, 1921-1926.

Johnson, K.M. & Segall, P., 2004. Viscoelastic earthquake cycle models with deep stress-driven creep along the San Andreas fault system. *J. Geophys. Res. Solid Earth*, 109, 1-19. doi:10.1029/2004JB003096.

Johnson, K.M., Bürgmann, R. & Freymueller, J.T., 2009. Coupled afterslip and viscoelastic flow following the 2002 Denali Fault, Alaska earthquake. *Geophys. J. Int.*, 176, 670-682. doi:10.1111/j.1365-246X.2008.04029.x.

Kenner, S.J. & Segall, P., 2003. Lower crustal structure in northern California: Implications from strain rate variations following the 1906 San Francisco earthquake, *J. Geophys. Res.*, 108. doi:10.1029/2001JB000189.

Kirby, S.H. & Kronenberg, A.K., 1987. Rheology of the Lithosphere: Selected Topics. *Rev. Geophys.*, 25, 1219-1244.

Lawson, C.L. & Hanson, R.J., 1995. Solving least Squares Problems, SIAM.

Marone, C.J., Scholz, C.H. & Bilham, R., 1991. On the mechanics of earthquake afterslip, *J. Geophys. Res.*, 96, 8441-8452.

Meade, B.J., 2007. Algorithms for the calculation of exact displacements, strains, and stresses for triangular dislocation elements in a uniform elastic half space, *Computers and Geosciences*, 33, 1064-1075. doi:10.1016/j.cageo.2006.12.003.

Nur, A. & Mavko, G., 1974. Postseismic Viscoelastic Rebound, *Science*, 183, 204-206. doi:10.1126/science.183.4121.204.

Okada, Y., 1992. Internal deformation due to shear and tensile faults in a half space, *Bull. Seismol. Soc. Am.*, 82, 1018-1040.

Peltzer, G., Rosen, P., Rogez, F. & Hudnut, K., 1998. Poroelastic rebound along the Landers 1992 earthquake

surface rupture. *J. Geophys. Res.*, 103, 30131-30145. doi:10.1029/98JB02302.

Perfettini, H., Avouac, J.P. & Ruegg J.C., 2005, Geodetic displacements and aftershocks following the 2001 Mw = 8.4 Peru earthquake: Implications for the mechanics of the earthquake cycle along subduction zones, *J. Geophys. Res. Solid Earth*, 110, 1-19. doi:10.1029/2004JB003522.

Pollitz, F.F., 1997. Gravitational viscoelastic postseismic relaxation on a layered spherical Earth. *J. Geophys. Res.*, 102, 17921-17941. doi:10.1029/97JB01277.

Pollitz, F.F., 2003. Transient rheology of the uppermost mantle beneath the Mojave Desert, California, *Earth Planet Sci. Lett.*, 215, 89-104. doi:10.1016/S0012-821X(03)00432-1.

Pollitz, F.F., 2005. Transient rheology of the upper mantle beneath central Alaska inferred from the crustal velocity field following the 2002 Denali earthquake, *J. of Geophys. Res. Solid Earth*, 110, 116. doi:10.1029/2005JB003672.

Riva, R.E.M. & Govers, R., 2009. Relating viscosities from postseismic relaxation to a realistic viscosity structure for the lithosphere. *Geophys. J. Int.*, 176, 614-624. doi:10.1111/j.1365-246X.2008.04004.x.

Rollins, C., Barbot, S. & Avouac, J-P. 2015, Postseismic Deformation Following the 2010 Mw7.2 El Mayor-Cucapah Earthquake: Observations, Kinematic Inversions, and Dynamic Models, *Pure Appl. Geophys.*, doi:10.1007/s00024-014-1005-6.

Rybicki, K., 1971. The elastic residual field of a very long strike-slip fault in the presence of a discontinuity, *Bull. Seism. Soc. Am.*, 61, 79-92.

Savage, J. & Prescott, W., 1978. Asthenosphere readjustment and the earthquake cycle, *J. Geophys. Res.*, 83, 3369-3376.

Savage, J.C. & Svarc, J.L., 1997. Postseismic deformation associated with the 1992 Mw=7.3 Landers earthquake, southern California rupture, *J. Geophys. Res.*, 102, 7565-7577.

Savage, J.C., Svarc, J.L. & Yu, S.B., 2005. Postseismic relaxation and transient creep, *J. Geophys. Res. Solid Earth*, 110, 1-14. doi:10.1029/2005JB003687.1.

Segall, P., 2010. Earthquake and volcano deformation, pp 185-186, Princeton University Press.